NMR IN BIOMEDICINE
NMR Biomed. 2006; **19**: 765–780
Published online in Wiley InterScience
(www.interscience.wiley.com) DOI:10.1002/nbm.1100

Clinical ultrashort echo time imaging of bone and other connective tissues†

Matthew D. Robson[1] and Graeme M. Bydder[2]*

[1]Oxford University Centre for Clinical Magnetic Resonance Research, OCMR Unit, John Radcliffe Hospital, Oxford OX3 9DU, UK
[2]The Department of Radiology, University of California San Diego, USA

Received 20 June 2006; Revised 9 August 2006; Accepted 9 August 2006

ABSTRACT: The background underpinning the clinical use of ultrashort echo time, SPRITE and other pulse sequences for imaging bone and other connective tissues with short T_2 is reviewed. Features of the basic physics relevant to UTE imaging are described, including the consequences when the radiofrequency pulse duration is of the order of T_2 so that rotation of tissue magnetization into the transverse plane is incomplete. Consequences of the broad linewidth of short T_2 components are also discussed, including partial saturation by off-resonance fat suppression pulses as well as those used in multislice and multiecho imaging. The need for rapid data acquisition of the order of T_2 is explained. The basic two-dimensional UTE pulse sequence with its half excitation pulse and radial imaging from the centre of *k*-space is described, together with options that suppress fat and/or reduce the signal from long T_2 components. The basic features of SPRITE and other sequences with very short *TE* are described. Image interpretation is discussed. Clinical features of the imaging of cortical bone, tendons, ligaments, menisci, periosteum and the spine are illustrated. The source of the short T_2 signal in these tissues is predominantly collagen and water tightly bound to collagen. Short T_2 components in all of these tissues are detectible and may show high signals. Possible future developments are outlined, as are technical limitations of clinical magnetic resonance systems. Copyright © 2006 John Wiley & Sons, Ltd.

KEYWORDS: magnetic resonance imaging; ultrashort echo time; pulse sequences; cortical bone; connective tissue; short T_2 tissues

INTRODUCTION

The most common clinical approach for diagnosis of parenchymal disease with magnetic resonance (MR) imaging is the use of heavily T_2-weighted pulse sequences to detect the signal from long T_2 relaxation components in normal tissue and an increase or decrease in the signal from these components in abnormal tissue. Even with newer pulse sequences such as fast spin echo, echo planar imaging, fluid-attenuated inversion recovery and diffusion-weighted imaging, the main diagnostic emphasis is on detecting the signal from normal and abnormal tissues with long T_2.

From the earliest days of clinical MR imaging it was recognized that there were also tissues such as cortical bone that had short T_2 (1,2). The MR signal from these tissues characteristically decays very rapidly, so that, with the echo times (*TE*) used with conventional clinical pulse sequences, little or no signal is detectable. As a result, these tissues appear dark.

The low or zero signal from cortical bone and other tissues with short T_2 provides a useful background against which to recognize abnormalities which increase T_2 sufficiently to result in a detectable signal. However, the absence of a signal in the normal tissue means that there is little opportunity to manipulate conspicuity by using different pulse sequences or contrast agents. It has not been possible to characterize these tissues in MR terms by measuring their T_1 and T_2 and assessing perfusion. Also, it may not be possible to differentiate between different tissues with short T_2, since each of the tissues produces the same very low or zero signal.

While tissues such as cortical bone, tendons, ligaments and menisci contain a majority of short T_2 components, other tissues such as skeletal muscle also contain short T_2 relaxation components, but as a minority species. A signal

**Correspondence to:* G. M. Bydder, Department of Radiology, University of California San Diego, 200 West Arbor Drive, San Diego, CA 92103-8226, USA.
E-mail: gbydder@ucsd.edu

Abbreviations used: 2D, two-dimensional; 3D, three-dimensional; CSI, chemical shift imaging; CT, computed tomography; FID, free induction decay; FT, Fourier transform; ADC, analog-to-digital converter; MIOP, magnetic iron oxide particle; MR, magnetic resonance; MT, magnetization transfer; SPI, single-point imaging; SPRITE, single-point ramped imaging with T_1 enhancement; rf, radiofrequency; T_1, longitudinal relaxation time; T_2, transverse relaxation time; T_2^*, transverse relaxation including effects due to field inhomogeneity; *TE*, echo time; TELEX, T_2-selective radiofrequency excitation; *TR*, repetition time; UTE, ultrashort echo time.

†This paper is published as part of a Special Issue entitled ''NMR of the Musculoskeletal System''.

Copyright © 2006 John Wiley & Sons, Ltd.

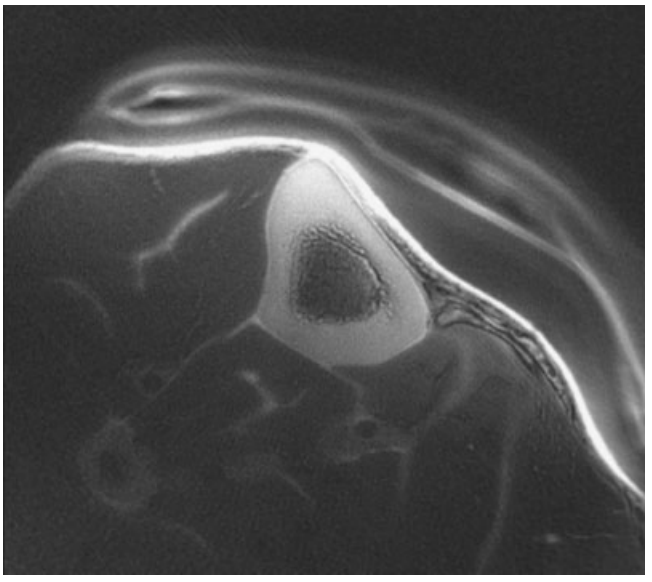

Figure 1. Transverse image of a normal tibia. Inversion recovery UTE image (*TR/TE/TI* 500/0.08/200 ms) image with magnitude reconstruction. The cortical bone is highlighted. Cortical bone has a shorter T_1 (130 ms) than any other tissue in the image. A signal is seen from the coil outside the leg

from the short T_2 components in these tissues is not directly detectable with conventional clinical pulse sequences. The MR signal comes from the majority of long T_2 components.

In quantitative terms, using conventional 2D Fourier transform (2DFT) imaging with basic clinical spin echo imaging sequences (with *TE* down to about 8–10 ms), tissues with T_2 shorter than 10 ms have not generally been detectable with clinical MR imaging in the past (3), although with the shorter *TE* in the range of about 1–2 ms now achievable with fast 2DFT gradient echo pulse sequences, the clinical limit of delectability is probably closer to 1–2 ms.

Two-dimensional pulse sequences with even shorter *TE* in the range 8–200 μs can be produced by using half radiofrequency (rf) excitations with radial mapping from the center of *k*-space (4–42). These ultrashort *TE* (UTE) pulse sequences have *TE* 10–200 times shorter than the shortest generally available on modern clinical systems. With these sequences, cortical bone can be visualized with a high signal in spite of its very short T_2 of 0.42–0.50 ms (Fig. 1). What applies to cortical bone also applies to other tissues with a majority of short T_2 components. In addition, using UTE pulse sequences, a signal can be specifically detected from the short T_2 components in tissues in which they are in a minority. For reference, ranges of *TE* with different pulse sequences are listed in Table 1.

Although the potential of UTE sequences has been apparent for many years, only a limited number of clinical studies of the lung and knee were published until quite recently. Less than 20 patients were reported in the 12 years following their first introduction in 1991. Studies have now completed of over 400 patients with this technique, and this experience has been used to review the background underpinning their clinical use in the musculoskeletal systems. Other sequences with short *TE*, such as single-point ramped imaging with T_1 enhancement (SPRITE), are on the verge of entering the clinical domain, and these are also discussed.

MR PROPERTIES OF TISSUE

Human tissue consists of multiple cell types that each contain multiple compounds, and these compounds typically include protons. As the T_2 of a species depends on the bonding and local neighborhood of atoms, it would come as a surprise if all the protons in a particular tissue demonstrated the same T_2, although this is the usual implicit assumption in MR imaging. This assumption is justified by the fact that the dominant MR signal in many tissues comes from compartmentalized water in cells and the extracellular space, and this exhibits monoexponential decay consistent with T_2 values of around 20–200 ms.

The more complex concept of tissue does point to the reality of the MR signal. Multiexponential decays have been demonstrated in detail in tissues such as nerve fibers (43,44) that have several different T_2 relaxation components even within the conventionally visible MR range ($10\,\text{ms} < T_2 < 300\,\text{ms}$), but it should not come as a surprise that there are also MR T_2 relaxation components that are outside the T_2 relaxation ranges that are visible with conventional MR. The range of T_2 visible with conventional MR imaging methods extends over about

Table 1. Approximate range of pulse sequence echo times (*TE*)

TE description	*TE* values	Examples[a]
Very long	200 ms and longer	2 DFT, fast spin echo and EPI; very heavily long T_2 weighted
Long	20–40 to 200 ms	2 DFT, HASTE, FLAIR, fast spin echo, EPI; heavily long T_2 weighted
Intermediate	5–10 to 20–40 ms	2 DFT; T_1 weighted or proton density weighted
Short	0.5 to 5–10 ms	2 DFT; T_1 weighted
Ultrashort	0.008 to 0.50 ms	Half rf pulse with radial center-out sampling; (UTE), pulse acquire, UTE-CSI, SPRITE

[a]The weighting depends on the T_1 and T_2 of the tissue or fluid of interest. EPI = echo planar imaging; FLAIR = fluid attenuated inversion recovery.

Copyright © 2006 John Wiley & Sons, Ltd.

DOI: 10.1002/nbm

Table 2. Approximate mean proton T_2 of some short T_2 tissues and tissue components[a]

Tissue or tissue component	Mean T_2
Periosteum	5–11 ms
Deep layers of articular cartilage	5–10 ms
Knee menisci	5–8 ms
Ligaments	4–10 ms
Achilles tendon	0.25 and 0.7 ms, 1.2 ± 0.2 ms, 0.53 ms (88%) and 4.8 ms (12%), 7 ms
Cortical bone	0.4–0.5 ms
Dentine	0.15 ms
Dental enamel	70 μs
Protons in water tightly bound to proteins	10 μs
Protons in proteins	10 μs
Protons in solids, e.g. calcium hydroxyapatite	1 μs or less

[a]The sources are adult clinical results and tissue sample results estimated for 1.5 T. Tissues with long T_2 such as nasal sinus mucosa that undergo significant dephasing may have short T_2^* (<10 ms) and thus appear similar to tissues with short T_2.

two orders of magnitude, and this can be stretched at the lower end by two further orders of magnitude with the use of UTE methods.

Table 2 lists the transverse relaxation times of a number of musculoskeletal tissues, and includes tissues that are visible with the UTE methods but are not detectable with conventional methods (i.e. $50\ \mu s < T_2 < 2$ ms).

For descriptive purposes, all tissues can be divided into those with a majority of short T_2 components, such as those in Table 3 and those with a minority, which includes tissues other than those listed in Table 3. The tissues with a majority of short T_2 components can be subdivided into cortical bone, dentine and enamel (very short T_2 and always a zero signal with conventional sequences), as well as other tissues with T_2 components that are not quite as short and that show a low signal (but not always a zero signal) with conventional sequences. The many tissues with a minority of short T_2 components, such as skeletal muscle, have these components present in low concentrations, typically of about 1–20% (45).

Table 3. Normal (adult) tissues with a majority of short T_2 components

Bone	Very short Dentine	Enamel
	Short	
Meninges (dura)	Falx	Tentorium
Membranes	Capsules	Bands
Retinaculi	Septae	Fascae
Sheaths	Nails	Hair
Aponeuroses	Tendons	Ligaments
Menisci	Labrii	Periosteum

It should be noted at this point that, although the T_2 components of these species are short, the T_1 behaviour of these species is not always as long as that found in crystalline solids. This is perhaps surprising, as it is well known that solids typically exhibit both short T_2 and extremely long T_1. Many of the T_1 for these components are in the 200–500 ms range, which makes them shorter than typical T_1 of tissues observed *in vivo* (the exception being fat).

Not all short T_2 components have the short T_1 described above. For example, phosphorus in bone is visible with UTE methods, displaying a T_2 of the order of 200 μs but T_1 of around 10 s, which is more representative of a typical crystalline solid (28). Further, some UTE effects are T_2^* and not T_2 effects, and in this case the T_1 will be representative of the material upon which the magnetic field inhomogeneity is acting. For example, tiny regions of paramagnetic material (e.g. after tiny bleeds within the brain) will display short T_2^* in the tissue surrounding the blood, but the T_1 in this surrounding tissue may not differ from its normal T_1. Both of the above cases are considered as special cases in the context of the musculoskeletal system, and collagen will be focused upon.

Collagen is important in the context of short T_2. It is a macromolecule that pervades the human body. It exists in bone, tendons, ligaments and other connective tissues, providing a key tensile component within the skeletal system. Several different types of collagen have been characterized histologically, as would be expected from the diverse use that the body makes of this macromolecule, although each of these types of collagen have similar molecular structures. Collagen has been studied extensively, and its anisotropy and structure combine to give it interesting MR characteristics. Collagen may display strong magic angle behaviour owing to the uniform orientation of the collagen fibers and the restricted motion of the protons associated with these fibers (46–50). This magic angle phenomenon has been used to examine the structure of the collagen itself (51,52). Collagen has multiple relaxation components that depend on the hydration of the collagen. In tendons these different relaxation components provide additional information about the structure of the collagen, suggesting that the protons in the cleft of the collagen have short T_1 and are in rapid exchange with the other protons and hence act as a relaxation sink for the collagen. A similar situation is found in bone (52), where rapid exchange of magnetization is found between the solid pool of protons (associated with the backbone of the collagen) and the hydrogen-bonded protons of collagen.

MR OF SHORT T_2 TISSUES

The MR theory of short T_2 species is no different to standard MR theory, but the short T_2 regime requires

Copyright © 2006 John Wiley & Sons, Ltd.

DOI: 10.1002/nbm

a fresh look at some concepts that are often taken for granted. The effects of relaxation while rf pulses are played out is often ignored. When the T_2 is >10 times the pulse duration any such effect is insignificant, but with shorter T_2 species these effects can be considerable. Further, the effects of relaxation during the signal acquisition period are normally only of concern with multiple-echo sequences, but those in the short T_2 regime need also to be reassessed. Finally, the complex effects of off-resonant saturation are generally only a concern when thinking about magnetization transfer (MT) effects (53), but these need to be re-evaluated for short T_2 components.

Relaxation during rf pulses

When the T_2 is comparable with the duration of the excitation pulse, it is necessary to consider how T_2 affects the resultant magnetization. In this situation, relaxation during the rf pulse results in reduced transverse magnetization and decreases the change in longitudinal magnetization induced by the rf pulse. These effects can be evaluated using a Bloch equation simulation with a time step that is short compared with the T_2. The effect of a 3 ms 90° Gaussian excitation pulse is simulated for different T_2 species in Fig. 2. The consequence of relaxation during rf pulses also has implications for refocusing and inversion pulses. On high-field (i.e. 1.5 T and greater) whole-body imaging systems it is typically not possible to play out a 180° pulse in a time much less than 500 μs, and hence this places a practical limit on how these pulses can be used (indeed, the magnetization of a tissue with T_2 of 200 μs cannot be inverted or refocused with such a system). This limit also has consequences for inversion recovery methods, adiabatic pulses and spin echoes which, as a consequence, are all challenging techniques for short T_2 species.

The other effect of relaxation during rf pulses concerns the action of rf pulses that would normally not affect the spins of interest. Dark blood pulses such as a non-slice-selective pulse followed by a slice-selective pulse will have little or no effect on a long T_2 material, but the longitudinal magnetization of the short T_2 component will be partially saturated by each of these 180° pulses, and hence the signal from the short T_2 species will be reduced. A further consequence of the short T_2 is that these species are sensitive to off-resonant excitation. This type of excitation occurs with multislice imaging, fat saturation, MT pulses and outer-volume excitation pulses, and would usually be expected not to affect the spins of interest. The sensitivity to off-resonant excitation is similar to the mechanisms that are commonly utilized for MT contrast and relates to the broad linewidths of the short T_2 spectral peaks. For short T_2 species that can be imaged directly (i.e. $T_2 > 100$ μs) the effects are smaller than typical MT effects (typically $T_2 < 100$ μs) but still have a measurable impact on image signal intensities. Once again these effects can be evaluated using Bloch equation simulations.

This sensitivity of the different species to the rf pulse duration may be exploited by purposely using pulses of long duration selectively to rotate long T_2 components

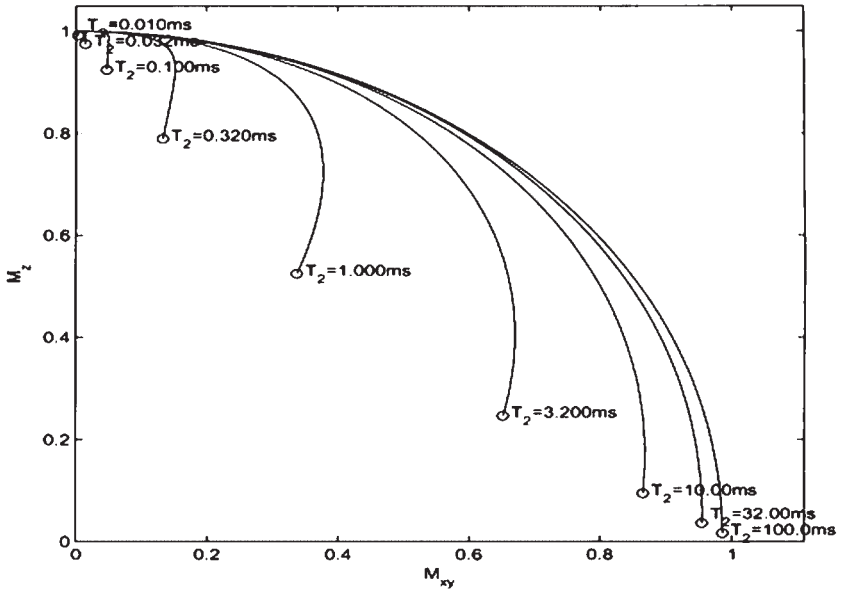

Figure 2. Simulation of the magnetization trajectory during a 3 ms 90° Gaussian (FWHM = 2 ms) pulse, showing rotation of longitudinal magnetization M_z into the transverse plane to become M_{xy} for tissue T_2 between 0.01 and 100 ms and T_1 of 1 s. For a tissue with $T_2 = 100$ ms, rotation is almost complete, but, as T_2 is decreased, less magnetization is rotated until, for $T_2 = 0.01$ ms, there is virtually no magnetization rotated into the transverse plane. M_z is also reduced

Copyright © 2006 John Wiley & Sons, Ltd.

DOI: 10.1002/nbm

into the transverse plane but leave short T_2 components largely unaffected. For example, to reduce the signal from long T_2 components, a long-duration (e.g. 10 ms) rectangular 90° pulse may be used to rotate the long T_2 components into the transverse plane and then dephase these components with crusher gradients while leaving the short T_2 components largely unaffected (54).

While it can be very difficult to invert short T_2 components, it is much easier to saturate them. To do this they need to be excited, but the dephasing process is then very effective and very short T_2 components may not even need a subsequent dephasing gradient pulse. As a result, methods of measuring T_1 of short T_2 components that include inversion pulses are fraught with difficulty, while those utilizing saturation pulses are relatively straightforward.

The distinction between T_2 and T_2^*

The distinction between T_2 and T_2^* is relevant when considering species that relax very quickly. T_2 is the spin–spin relaxation time, whereas T_2^* is the relaxation time observed with a gradient echo pulse sequence and includes both T_2 relaxation and coherent dephasing effects which are highly dependent on the imaging technique used. Dephasing effects arise from spins within a voxel having different precession frequencies owing to local field variations. The difference can be strongly affected by the voxel dimensions. This intravoxel dephasing may be reduced to a level where it is insignificant if *TE* is decreased from conventional values of 10 ms to 0.1 ms or less. Dephasing effects due to factors such as poor shimming or inhomogeneity in large voxels at air–tissue interfaces are reduced. T_2 and T_2^* are differently affected by excitation pulses, and it may be possible to exploit this to separate out these two phenomena. Without a spin echo method it is difficult to prove that the T_2^* values measured represent the T_2 value, but in materials with no known dephasing sources it is reasonable to assume that the measurement essentially reflects T_2, while in other tissues (for example cortical bone, or around regions of paramagnetism) it is necessary to be more cautious as dephasing effects may be affecting the signal.

Data acquisition

Finally, and perhaps most obviously, when imaging short T_2 tissues, the data must be acquired soon after the signal has been excited. This requirement is true both for the center of *k*-space, which determines the contrast of the image, and for the periphery of *k*-space. The decay of the signal during data acquisition can result in the loss of high-resolution detail since the amplitude of the signal may be low or zero when the outer regions of *k*-space are sampled (36,37).

SHORT *TE* PULSE SEQUENCES

Pulse acquire

The free induction decay (FID) of the pulse acquire experiment provides the simplest method for observing short T_2 components. With this method, the only limitation is the time between playing out the rf pulse and sampling the signal. This approach and methods that use additional refocusing pulses have the benefit of producing the shortest practical T_2^* and T_2 weighting and are routinely used on high-resolution spectroscopy equipment. The obvious disadvantage of these methods is that they provide little or no localization. This is limited to rf localization methods (e.g. transmit field modulation methods) and so far has had little *in vivo* applicability.

CSI and UTE-CSI

The next level of simplicity is to apply the same short rf pulse, but then follow this with phase-encoding gradients to provide spatial sensitivity as with chemical shift imaging (CSI) (55). If a slice selection gradient is not used, then the need for slice selection and refocusing gradients can be avoided, and three-dimensional phase encoding can be used. In this case the minimum time between excitation and acquisition (the T_2^* weighting) is limited by the time required to play out the longest of the phase-encoding gradients, and hence depends on the resolution of the image. For low-resolution images and high-performance gradient systems this can be as short as a few 100 μs.

The ultrashort *TE* [UTE-CSI (42)] variant of the CSI method is a simple modification of this approach that uses the same excitation and 3D phase-encoding scheme, but each phase-encoding gradient is designed to be as brief as possible. After each phase-encoding gradient is completed, samples are immediately collected. The consequence of this is that the central *k*-space points have much smaller degrees of T_2^* weighting than the edges of *k*-space. The contrast on the images depends on the centre of *k*-space, with the edges of *k*-space providing resolution information. This approach has been demonstrated to be useful for tissues and with T_2 as short as 180 μs on clinical MR imaging systems (28).

The advantage of CSI approaches is that they provide four-dimensional data with the whole signal decay sampled over all of *k*-space. The disadvantage of these approaches is that, owing to the three dimensions of phase encoding, they require a great deal of time when used at anything other than low resolution, although this problem can be alleviated to some extent by using large arrays of small rf coils.

SPI and SPRITE

Single-point imaging (SPI) (56,57), also known as constant-time imaging (CTI), and the more recent

Copyright © 2006 John Wiley & Sons, Ltd.

DOI: 10.1002/nbm

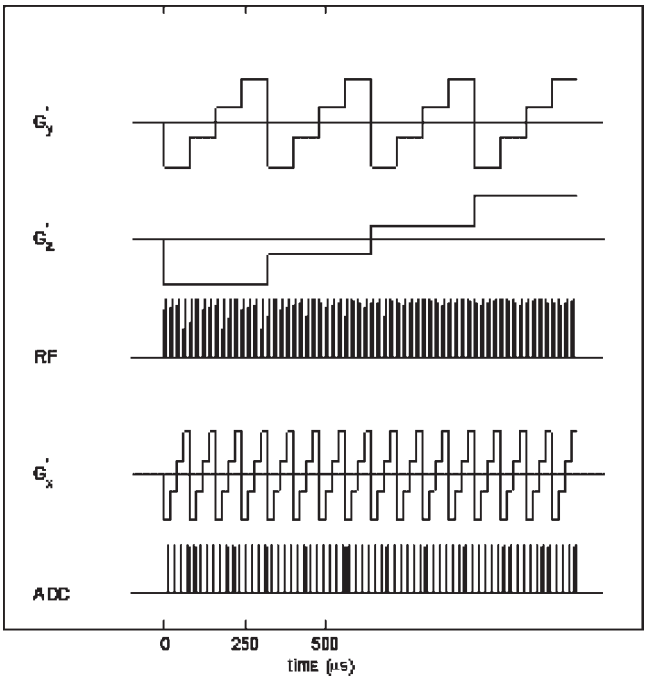

Figure 3. Pulse sequence diagram for SPRITE sequence (a) showing a schematic sequence with only a $4 \times 4 \times 4$ imaging matrix. Typical acquisitions have matrix dimensions in excess of 64, with much longer acquisition times. The first two lines of phase encoding are shown (b), demonstrating the small steps required in gradient switching, and the short rf pulses that are required

single-point imaging with T_1 enhancement (SPRITE) (58) use a similar 3D encoding approach but remove the problems and delays associated with rapid switching of magnetic field gradients. With the SPI sequences the imaging gradients are turned on prior to spin excitation, and a very short rf excitation pulse is used. The short rf pulse has a very wide bandwidth, and hence the imaging gradients have no effective slice selection and so the whole volume of the sample is excited equally regardless of the imaging gradient strength (Fig. 3). In order to sample 3D *k*-space, the imaging gradients follow certain trajectories. Figure 3 shows a raster sampling scheme, but centric and conical sampling schemes can be used with SPRITE which can decrease the amount of T_1 weighting at the centre of *k*-space. Different approaches can be used within this scheme, but the simplest variant uses the imaging gradients as phase-encoding gradients and samples just a single *k*-space point with each excitation. In this case each *k*-space point is sampled at the same time after excitation, and hence has the same T_2^* weighting. More complex variants (59) use the imaging gradients as a readout and sample more points either with rapid gradient switching or without. It is also possible to use swept radiofrequency excitation (60).

The advantage of the SPI methods is that they provide the lowest degree of T_2 weighting of any imaging sequence, as there are no delays due to gradient switching and hence *k*-space is traversed as quickly as possible with the available gradient system. The expected disadvantage of SPI is that it is a 3D approach and hence requires long imaging times, but in practice this may not be a serious problem, as short (e.g. 100 μs) *TR* can be used with this sequence. For example, with a *TR* of 100 μs at $256 \times 256 \times 128$ matrix size, the acquisition would take only 14 min, and elliptical sampling methods could shorten this. The SPRITE sequence in its basic form is a spoiled gradient echo, which is primarily T_1 weighted, but a magnetization preparation pulse may be used before the SPRITE readout in order to superimpose additional weightings on the image. Segmented acquisitions are required with these approaches. Various methods have been developed for this type of characterization (61,62). The low peak B_1 presently available on whole-body clinical MR systems may limit the utility of SPRITE methods, but human *in vivo* measurements have been made (63).

UTE sequence

It is possible to shorten *TE* and avoid the need for rephasing of the slice-selective rf excitation pulse by first collecting the data with the slice selection gradient in one direction and adding this to data collected in the same way with the slice selection gradient reversed (Fig. 4). In this way, data sampling can, in principle, begin as soon as the rf pulse and the slice selection gradient are ramped down to zero. The use of radial imaging of *k*-space with the acquisition starting in the center of *k*-space (where no gradient is required for the initial encoding) means that there is no need for a phase-encoding gradient, a read-dephasing gradient or additional readout time to return to the center of *k*-space in the read direction. Data sampling can continue while the gradient is being ramped up (although sampling during ramping takes a longer time than when the gradient is fully ramped up), as well as after the gradient has reached its plateau (Fig. 5). The gradient also needs to be ramped down very quickly at the end of the rf excitation since persistence of the gradient after the end of the rf pulse may result in dephasing of the signal.

It is usual to take *TE* as the time from the mid-point of the rf excitation pulse to that of the sampling of the center point of *k*-space. This is appropriate (or only slightly in error) for long T_2 components, but the precise value of *TE* may become uncertain with short T_2 components (64,65). It can be shown that for long T_2 species the center of mass of the rf pulse provides the reference from which *TE* should be determined even for a half pulse excitation. In the case of short T_2 components, this center of mass calculation needs to be weighted by the effective memory that the spin has of the pulse. The calculation is modified by weighting the center of mass calculation with an exponential relaxation term with the T_2 of the species as the decay constant (65). Unfortunately, this results in a *TE* that depends on T_2 and is complex to determine.

Copyright © 2006 John Wiley & Sons, Ltd.

DOI: 10.1002/nbm

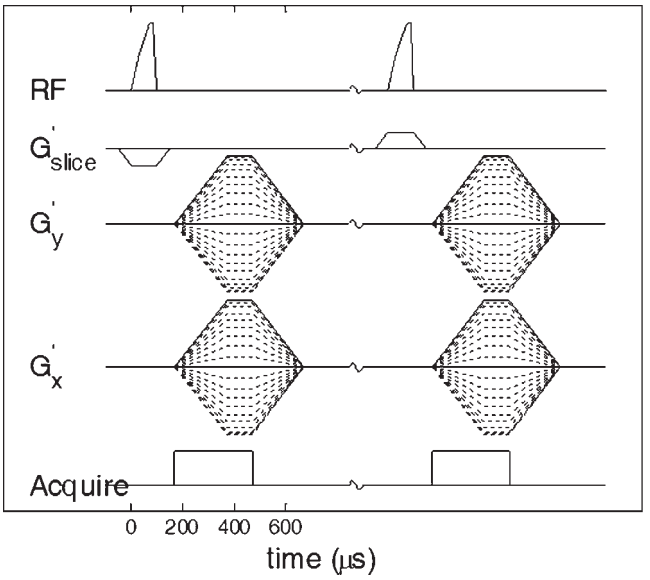

Figure 4. Pulse sequence diagram for a basic UTE sequence. The half rf pulses are applied with the slice selection gradient G_z negative in the first half and with this gradient positive in the second half. The rf pulse is truncated and followed rapidly by the acquisition during which G_x2 and G_y2 are applied to give the radial gradient. These gradients ramp up to a plateau during data acquisition

Consequently, the end-point of the rf excitation has become a popular reference point from which *TE* is measured, although this approach can result in spuriously short values for *TE*.

The UTE pulse sequence is not a spin echo or gradient recalled echo (since reversed gradients are not used to form an echo). The FID is directly detected. There is no echo since the signal is not refocused and each half-

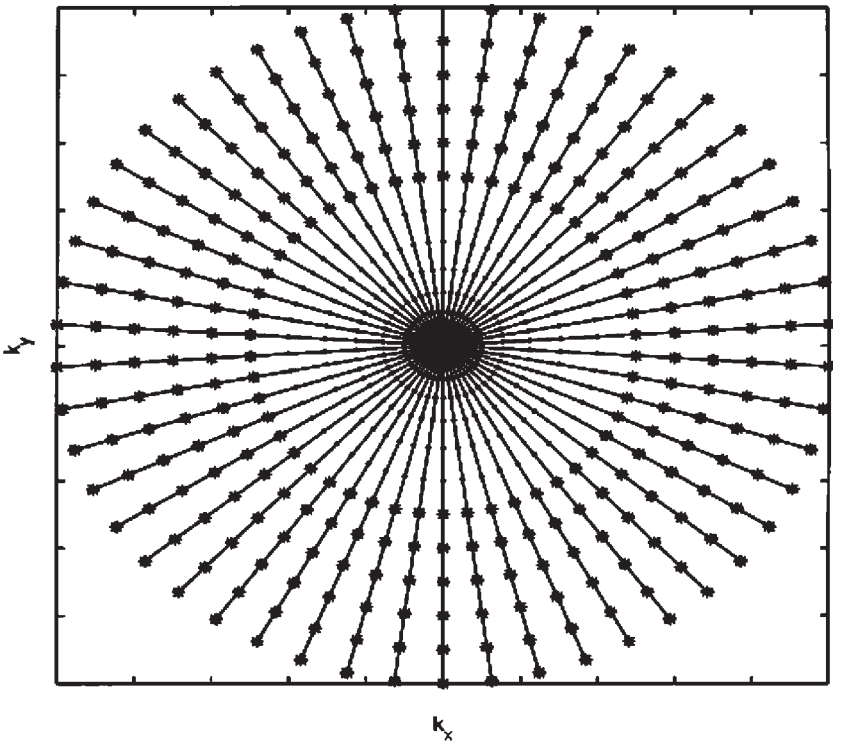

Figure 5. *k*-Space trajectories for the above imaging sequence. Each 'spoke' represents the *k*-space trajectory due to the readout gradients. The dots represent the central points which are sampled on the gradient ramps, and the stars the peripheral points which are sampled on the gradient plateau. Practical acquisitions typically include 128–512 spokes and 256–512 points on each spoke. The data points are regridded onto a Cartesian grid prior to 2D Fourier transformation

Copyright © 2006 John Wiley & Sons, Ltd.

DOI: 10.1002/nbm

excitation is not fully rephased. It is only after the pair of excitations is added that the *k*-space data are in phase.

While simple UTE sequences are effective for imaging tissues with a majority of short T_2 components, some form of long T_2 component reduction is necessary selectively to image short T_2 components in tissues in which they are a minority. The initial approach to this problem was to use a long (e.g. 10 ms) rectangular 90° pulse followed by a dephasing gradient, as explained previously. The TELEX approach (66) performs the same function as this by saturation of the long T_2 components. Another method involves the use of an initial long inversion preparation pulse (e.g. 4 ms) selectively to invert long T_2 components followed by a T_1 chosen to null them. This technique requires knowledge of the T_1 of the long T_2 components. A third method is to subtract a later echo image from the first (UTE) image and produce a difference image. Tissues or fluids with a long T_2 have their signal attenuated by this procedure, while tissues that have a short T_2 and decay rapidly between the two echoes are highlighted on the resulting difference image. The disadvantage of this differencing approach is that the difference image is sensitive to susceptibility artifacts. T_2 suppression methods are the subject of ongoing investigation (38,40).

Pulse sequences employing half rf pulses and radial sampling were first implemented for clinical purposes by Bergin *et al.* from Stanford in 1991 and 1992 (4,5) and were initially applied to lung imaging. This implementation incorporated spectroscopic imaging and a modified Dixon technique for separation of fat and water signals, as well as a 90° rectangular preparation pulse for suppression of long T_2 components. Musculoskeletal applications followed in 1995 (7). Half rf excitations have been implemented with center-out radial mapping of *k*-space with *TE* of 0.07 or 0.08 ms but in a more modular form, details of which are given below.

Truncated rf pulses of 0.40–0.50 ms duration are used with slice-selective gradients applied in one direction and then reversed for the second half of the acquisition. The two sets of data are added to give a single radial line of *k*-space, and the process is repeated through 360° in 128–512 steps. The data are mapped onto a 512×512 grid and reconstructed by 2D Fourier transformation. Four sets of images with equally spaced *TE* (0.08, $0.08 + t$, $0.08 + 2t$, $0.08 + 3t$ ms), typical spacings t are 2.79 ms (at 2 μs per sample) or 6.62 ms (at 4 μs per sample), are usually obtained, which allows the creation of composite images with different T_2 sensitivity by subtracting each of the three later echo images from the UTE image. Spacings of 4.7 ms at 1.5 T allow the fat and water to remain in phase for all acquisitions, which can be beneficial. The length of the ADC sample window dwell time during the acquisition represents a compromise between minimizing T_2 decay and maximizing SNR. Data are usually sampled over 256–512 points. Slice selection in multislice sets is performed with sequential excitations with the positive gradient, followed by sequential excitations with the negative gradient. Contiguous multislice interleaved excitations may interfere directly with the half rf pulse since the slice profile of a half-pulse alone is spread out. Versions of the basic sequence with frequency-based fat suppression and/or long T_2 component suppression have been implemented. Initial short (0.40 ms) or long (4 ms) inversion pulses are used as preparation pulses. With each variant of the sequence, difference images formed by subtraction of subsequent echo images from the first echo image are produced. Fields of view of 12–40 cm are employed with slice thicknesses of 4–8 mm. *TR* of 500 ms are commonly used with UTE sequences with flip angles (for long T_2 components) of 45–80° and slice gaps of 10–100%. Serial studies of contrast uptake use a *TR* of 50–100 ms. Inversion recovery sequences have *TR* of 650–2500 ms. Breath-hold and cardiac-gated sequences use *TR* of 10 ms. Scan times vary from 12.8 s to 17 min.

MACHINE PERFORMANCE AND PRACTICAL LIMITS

One approach to the problem of imaging short T_2 species would be to use conventional imaging methods but to reduce the duration of the rf pulses so that they are short compared with T_2, and to play out readout gradients in times much shorter than the T_2. In this regime the effects of T_2-dependent signal decay would be minimized and conventional imaging sequences and methods could be used with impunity. This approach is possible on small-bore solid-state imaging systems, but not on human-sized systems.

Two elements act to limit the performance on whole-body human imaging systems:

1. The first is technical and includes the practical difficulties of building gradient systems with a 100-fold increase in performance compared with current systems (i.e. slew rates of 2 T/m/ms and peak gradients of 40 T/m), as well as rf systems capable of 10 μs 180° pulses (i.e. >500 kW rf amplifier peak power). These are the sort of improvements that would be required substantially to affect the T_2 regime to which humans are sensitive.
2. The second limit involves the human subject. Current maximum gradient switching guidelines are limited to <20 T/m/s, and rf excitation pulses are limited by heating limits (<4 W/kg instantaneous). Although there are ways to elevate these limits to some degree (perhaps by a factor of 2 or 3), the orders of magnitude increase in performance required to make the direct imaging of T_2 down to 5 μs is unlikely to be achievable on human systems.

Both the technical and safety limits are higher for systems that do not image the whole body and have a clear bore diameter of maybe 10–20 cm, and these could

Copyright © 2006 John Wiley & Sons, Ltd.

DOI: 10.1002/nbm

accommodate a hand or limb of the subject. In this case the technical limits may be surmountable, and it may prove possible to perform experiments of this sort within some acceptable safety framework in the future.

Switching time (from transmit to receive) has already been shortened to 8 μs on clinical systems (26) and can theoretically be shortened to <1 μs if the same coil is used for both transmission and reception. Excitation does not provide a fundamental limit as it is possible to play out short pulses with low excitation angles, and slice selection gradients do not limit the technique as it is always possible to use a 3D acquisition and localize using the field of view of the rf coil. It is the readout gradient and the requirement to get to high *k*-space points while a signal is present that provides the ultimate resolution limit.

It is possible to estimate the practical limit of T_2 that can be imaged in humans. A resolution requirement of 1 mm in plane, a peak gradient strength of 40 mT/m and a peak slew rate of 200 T/m/s and a need to play out a 40 μs rf pulse (10–15° given 1 kHz B_1 amplitude) are assumed. Further, to obtain a practical resolution, it is assumed that the acquisition must be completed before two T_2 have elapsed. Using these basic values, it is possible to show that the UTE readout requires some 150 μs; if this is added to the duration of an rf pulse of ~40 μs, and if there is no delay between excitation and sampling, the minimum visible T_2 is about 85 μs. If the gradient slew rate and peak strength are doubled, these values are only shortened to ~60 μs. At these short T_2 a severe obstacle is the ramp time (200 μs), and hence the UTE method is slew rate limited on clinical systems.

With SPRITE using the same specifications but a shorter rf pulse (1 μs to avoid slice selection effects over a 20 cm FOV, at ~0.4° given 1 kHz of B_1 power), it is possible to acquire data in about 60 μs (or 30 μs under the doubled gradient performance conditions), which will adequately image samples with T_2 of 30 or 15 μs respectively. If a 1° pulse were required, then this would limit the readout gradient (given this sample size) and increase the readout duration to ~170 μs. With SPRITE there is a strong trade-off between minimum sampling duration and SNR which becomes severe at short sampling times owing to the low peak B_1 available with clinical MR systems, and SPRITE is B_1 limited on these systems.

It is perhaps fortunate that there is so much signal from T_2 species in the range $100\ \mu s < T_2 < 5$ ms, as the shorter T_2 values are likely only to be demonstrable indirectly via exchange mechanisms (i.e. via MT).

CONTRAST ENHANCEMENT

Intravenous gadolinium chelates (e.g. gadodiamide 0.3 mmol/kg) may show enhancement in tissues with short T_2 using UTE sequences when this is not apparent with conventional sequences because no signal is detectable from them either before or after contrast administration. The effect results from a shortening of T_1 and may be of particular interest because some tissues with a majority of short T_2 components are avascular or relatively avascular, and contrast enhancement may allow perfusion and diffusion to be studied within them. The detection of normal enhancement in tissues with short T_2 may allow a reduction in this enhancement to be recognized in disease. Even in tissues where signals are detectable with conventional sequences, the signals from the majority of longer T_2 tissues may be detected earlier during their decay, and a signal from the minority of short T_2 components may also be detected. This may allow the tissue to be visualized with higher signal intensity before enhancement and to show a greater increase in signal after enhancement.

Another feature of interest with UTE sequences is that they may be able to detect signals from tissues with short T_2 and concurrently reduce or suppress signals from tissues or fluids with a long T_2. This can be achieved by using different long T_2 reduction techniques. This option may be useful with contrast enhancement with gadolinium chelates, where frequently the greatest change is seen in blood (which has a long T_2) but the area of most clinical interest may be adjacent or associated tissue with a short T_2.

Magnetic iron oxide particles (MIOPs) typically produce a loss of signal through susceptibility effects. This loss of signal may not be manifest with conventional sequences in tissues that produce no signal prior to enhancement, such as tendons and ligaments. In this situation the presence of these particles may be inferred by loss of signal in surrounding tissues or fluids that have detectable MR signals. The use of UTE sequences to produce a detectable signal in the tissues of interest may provide a baseline to recognize a reduction in this signal produced by MIOPs (39).

A particular problem with intravenous use of MIOPs is that they frequently produce a loss of signal in the area of most interest, which may make image interpretation difficult. This signal drop is due to shortening of the T_2 below the level to which conventional sequences are sensitive (gadolinium chelates, as most commonly used clinically, do the reverse, by increasing the signal in the area of most interest). Also, with the use of oral MIOPs to reduce the unwanted signal from bowel contents, the loss of signal may extend beyond the bowel and produce loss of signal in adjacent organs. UTE images typically show low sensitivity to susceptibility effects, but later echo images show higher sensitivity to these effects. Subtraction of a subsequent echo from the first produces a difference image in which the anatomic detail from the first (UTE) image is well preserved but modulated by the susceptibility-dependent contrast developed by the later echo, with a higher signal on the difference image representing a greater degree of susceptibility effect.

Copyright © 2006 John Wiley & Sons, Ltd.

DOI: 10.1002/nbm

IMAGE INTERPRETATION

The interpretation of UTE images follows established principles, but there are some interesting differences. The term 'T_2 weighted' as usually applied to a pulse sequence is generally taken to mean weighting for long T_2 components in a tissue or fluid by using a long *TR* and long *TE* pulse sequences. Sequences may also be *T2* weighted but for short T_2 components, i.e. with T_2 less than 10 ms, using short *TE* rather than long ones. For clarity, in situations where there may be confusion, it may be necessary to use the terms 'long T_2 weighted' and 'short T_2 weighted'. Sequences may be both short T_2 and T_1 weighted at the same time if they have a short *TE* and a short *TR*, or just short T_2 weighted if they have a short *TE* and long *TR* (relative to T_1).

As a rule, the T_2 weighting of a sequence is maximal for small increases or decreases in the T_2 of a tissue when its *TE* is about the same as the tissue T_2. Therefore, UTE sequences alone (e.g. $TE = 0.08$ ms) are not particularly T_2 weighted for most tissues in the short T_2 range since these tissues often have longer T_2. Although the T_2 weighting of UTE sequences is low for most short T_2 tissues, T_2 weighting increases for tissues in the short T_2 range with later echoes (e.g. with $TE = 2.87$, 5.66 and 8.45 ms). These may detect an increase or decrease in signal intensity in disease relative to normal tissue.

The long T_2 reduction techniques also effect T_2 weighting but in a different way. They selectively attenuate the signal from tissues with long T_2, leaving only the short T_2 components. As a result, the sequence only shows a signal from tissues with T_2 within a restricted range or window (Fig. 6). Tissues may enter or leave this window of visibility at either end by increasing or decreasing their T_2. The width of the window varies with the duration of the rectangular pulse, the length of the nulling inversion pulse and the *TE* of the subtracted echo.

UTE sequences are T_1 weighted if the *TR* is about the T_1 of the tissue of interest, with due allowance for flip angle. This is the common situation. With inversion recovery sequences, T_1 weighting is maximal if the T_1 is about the T_1 of interest, although this is only applicable for tissues with T_2 relatively long compared with the duration of the inversion pulse. Cortical bone has a T_1 in young and middle-aged subjects of 130–160 ms at 1.5 T, which is shorter than that of subcutaneous fat. The T_1 of cortical bone increases significantly with age to 260–280 ms in the ninth decade. Tendons, ligaments and menisci have relatively short T_1 in the range 300–600 ms at 1.5 T. T_1 of short T_2 components in tissues in which they are in a minority are less well characterized but are probably similar.

Conventional proton density weighted pulse sequences with typical *TR* of 2000–3000 ms and *TE* of 10–20 ms do not detect a number of short T_2 components which contribute to proton density as measured by chemical assay. Even UTE sequences do not detect extremely short T_2 components. However, changes in proton density may be a greater source of contrast when imaging with short T_2 components than is the case with long T_2 components.

Each of the long T_2 reduction techniques has advantages and disadvantages. Long T_2 component suppression with a long preceding 90° pulse and dephasing has the disadvantage that no unsuppressed image is available, but the advantage that susceptibility effects are not introduced by subtraction of a later echo. However, susceptibility effects may render the long narrow-bandwidth pulse ineffective and result in a high unsuppressed signal from long T_2 components. The long inversion pulse sequences with nulling of long T_1 components may be difficult to interpret owing to magnitude processing and concerns about whether the chosen T_1 is correct. Subtraction images increase the noise level and introduce susceptibility effects, but both the original images and the subtracted image are available for examination.

To show selectively short T_2 components, subtraction images must have an adequate signal-to-noise ratio. Thus, cortical bone may be obvious in a subtraction image when it is situated close to a surface coil but be of low signal on all sequences (including subtraction images) when examined at some distance away from the conductors of a body coil.

Magic angle effects in tendons and ligaments are manifest as a relative increase in signal on later echo images (owing to the longer T_2) and a relative decrease in signal on difference images. These can be seen in the anterior cruciate ligament on the femoral side of the posterior cruciate ligament, as well as at other sites.

The conspicuity of increased or decreased signal from short T_2 components within a tissue differs depending on

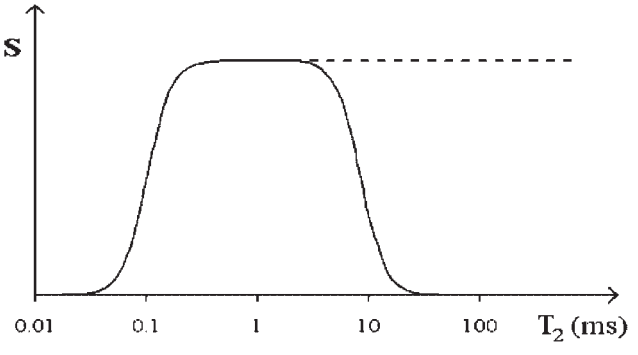

Figure 6. Stylized sensitivity profile of a UTE sequence to tissues with different T_2 shown on a logarithmic scale. The lower cut-off point is set by machine performance and is probably between 0.050 and 0.100 ms. Without T_2 reduction the sequence is sensitive to T_2 components in the range 1–10 ms and higher (dashed line). With T_2 reduction techniques the sensitivity to longer T_2 is reduced to zero (continuous line). There is thus a window of short T_2 to which UTE sequences with long T_2 reduction techniques are sensitive. Tissues can enter or leave this window of visibility by increasing or decreasing their T_2. The graph does not take into account differences in concentration of T_2 species or the effects of T_1, which both affect the detectable signal

Copyright © 2006 John Wiley & Sons, Ltd.

DOI: 10.1002/nbm

whether these components are in a tissue with a majority of short T_2 components or in a tissue with a minority of short T_2 components where the effect may be diluted unless the signal from long T_2 components is reduced. Likewise, the effect of a T_2 shortening process may be more obvious in a tissue with a minority of short T_2 components than in one with a majority where there are no long T_2 components available in the tissue to have their T_2 reduced.

Even when it is not necessary to reduce the signal from long T_2 components in a tissue of interest with a majority of short T_2 components to visualize them (e.g. tendons, ligaments, cortical bone), it may still be useful to do this in order to increase the conspicuity of these tissues by reducing the signal from other tissues with a minority of short T_2 components, such as muscle (see Fig. 1).

Diseases that increase the T_2 of tissues with a majority of short T_2 components may render them more obvious on later echo images but less obvious on difference images (i.e. the increase in T_2 takes them outside the visible window in Fig. 6). With conventional pulse sequences, contrast enhancement in these tissues (e.g. tendons and ligaments) may only be recognizable in areas where the T_2 is increased so that a signal is detectable. Paradoxically, with difference images, these may be just the areas where contrast enhancement is not visible on difference images because the increased T_2 leads to attenuation of the signal.

Particular artifacts associated with the use of UTE sequences include radial lines, susceptibility effects, out-of-slice effects, flow dephasing effects and effects due to delayed rf switching. Radial artifacts resemble those seen with CT. Susceptibility artifacts may be manifest as a high signal on difference images. However, within cortical bone they may produce a relative increase in signal on late echo images and have a low signal (rather than a high signal) within the bone on difference images, and may be a consequence of imperfect slice selection in regions of high field inhomogeneity. Out-of-slice artifacts can produce a high signal at boundaries or interfaces. Materials with short T_2 in the receiver coils often have a high signal. Large artifactual changes on difference images can arise from subtraction of later out-of-phase (fat and water protons) echo images from the first (UTE) image. Motion artifact is more prominent with later echoes and becomes more obvious on difference images. Flow of blood can lead to dephasing on the later echo images and a high signal on difference images, which simulates the signal from short T_2 components. Delay in coil switching and/or eddy currents may produce a mottled effect, and a relative reduction in the first echo compared with the second, with negative signals on difference images.

CLINICAL ILLUSTRATIONS

To date over 400 patients have been studied using the techniques described above. The selection of patient groups follows from a number of considerations. The detection of a signal from tissues with short T_2 that have previously been 'invisible' provides a new range of conspicuity options as well as new anatomic detail that has previously been undetectable. Pathologic processes that might either increase or decrease the signal from short T_2 components have also provided a guide for the use of UTE sequences. Applications in which conventional imaging has been relatively unrewarding but in which MT, MR spectroscopy or other imaging techniques have shown abnormalities have been another focus of attention.

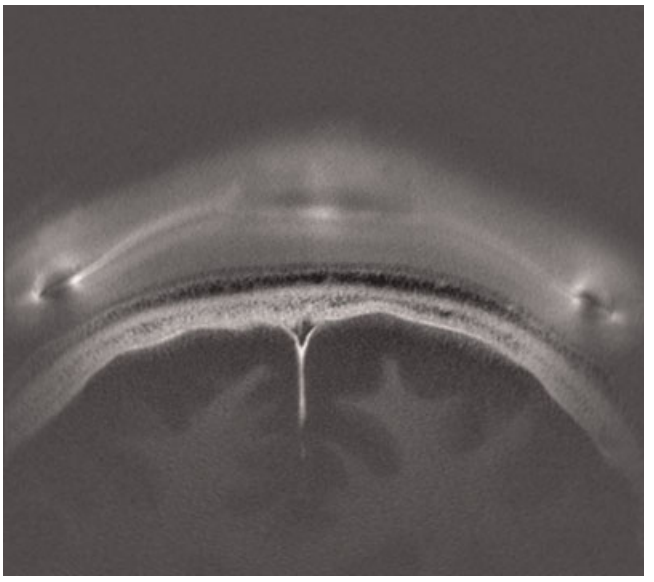

Figure 7. Frontal bone. Trabecular bone can be seen between the inner and outer tables

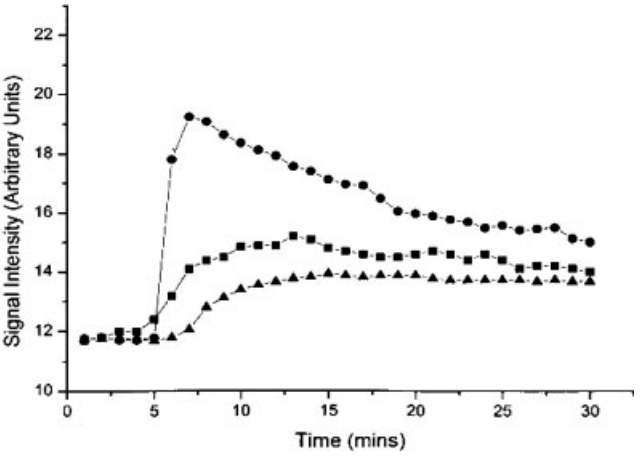

Figure 8. Signal intensities in cortical bone after fracture of the tibia. Intravenous gadodiamide was given after 5 min. Normal enhancement is shown by the triangles. Results in one patient 4 days after fracture (squares) are compared with those in another patient 3½ months after fracture (circles). There is a faster and higher increase in signal in the patient imaged 3½ months after his fracture

Copyright © 2006 John Wiley & Sons, Ltd.

DOI: 10.1002/nbm

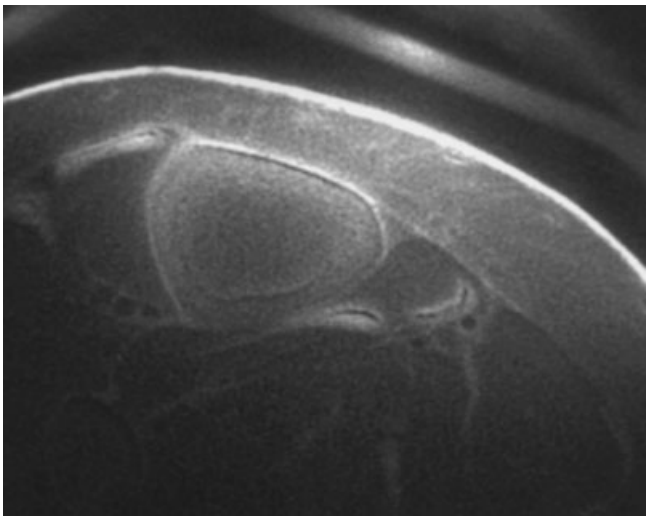

Figure 9. Osteoporosis: the tibia shows a much lower signal than in Fig. 1

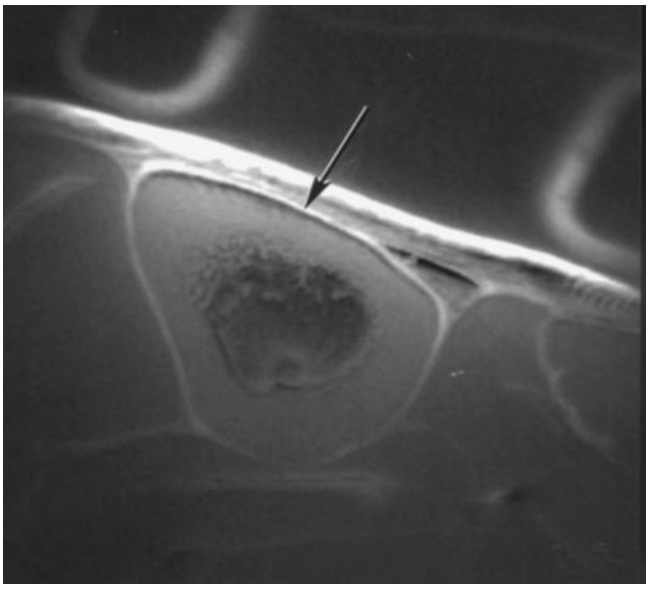

Figure 10. Normal periosteum. Transverse fat-suppressed difference UTE (*TR*/*TE* = 500/0.08 minus 5.95 ms) image. The periosteum (arrow) is highlighted

The proton signal from cortical bone probably comes mainly from the organic matrix (principally collagen), bound water and some free water. It may provide different information to conventional radiological methods which mainly reflect the calcium content of the mineral component. Trabecular bone can be seen (Fig. 7). Serial scanning shows enhancement in normal cortical bone. After intravenous gadodiamide there was a 23% increase in signal with a peak at about 10 min in the study illustrated, and this was greater following fracture (Fig. 8). The bone signal is reduced in osteoporosis (Fig. 9). The periosteum is well seen in many areas (Fig. 10), although there are other causes of high signal adjacent to cortical bone, and periosteum needed to be differentiated from these. Enhancement may be specifically demonstrated in the periosteum without the confounding effect of a high signal from blood by the use of subtraction.

A high signal was consistently seen in tendons and ligaments. Local enhancement may be seen (Fig. 11). A

Figure 11. Patella tendon: before (left) and after enhancement (right). Increased signal is seen in the tendon after enhancement (arrows)

Copyright © 2006 John Wiley & Sons, Ltd.

DOI: 10.1002/nbm

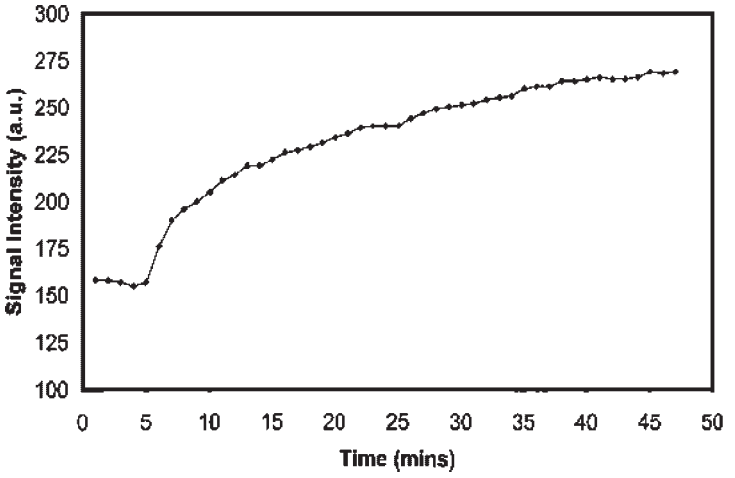

Figure 12. Plot of signal intensity before and after enhancement for a normal ACL. There is an increase in signal up to 40 min after injection

plot of signal intensity against time for the normal anterior cruciate ligament after contrast enhancement shows an increasing signal even after 40 min (Fig. 12).

The red (vascular) zone of the meniscus is well seen (Fig. 13). It has not been identifiable in previous studies in cadavers or patients (67).

Tendons and muscle insertions are highlighted. The signal may be from fibrocartilage (68) (Fig. 14).

Imaging of the spine shows an increased signal from ligaments and scar tissue and may show enhancement of abnormal discs (Fig. 15). Thalassemia is of interest as a condition in which there is premature intervertebral disc degeneration in the lower thoracic and upper lumbar spine. High-intensity bands can be seen parallel to the end plates, with fat-suppressed and long T_2 suppressed UTE sequences. These changes may be due to iron deposition shortening the T_2^* of the disc.

FUTURE DEVELOPMENTS

Many further developments are possible. The process of optimization of *TR*, flip angle and data sampling for different tissue T_1 and T_2 has only just begun. The same applies to the different long T_2 signal reduction techniques. In general, fast low-flip-angle techniques are likely to form the basic pattern for UTE imaging. The T_1 of short T_2 components (apart from phosphorus in bone) are generally short which assists with fast sequences. The technique is also well suited to low flip angles in order to keep rf pulse durations short.

The rf switching times are now as short as 8 μs (26,33). There are also options already available for use of increased B_1 power and gradient strength with smaller dedicated transmit–receive coils and gradient sets for imaging of the brain, knee and other parts of the body. These should allow shorter rf pulses and faster ramping to higher gradient strengths, which will improve image quality and further extend the window of visible T_2 species. Reversed radial sampling should improve the signal-to-noise ratio for later echoes but requires near-perfect gradient performance. Gradient moment nulling is likely to be of value in reducing motion artifact from later echoes.

Spiral acquisitions also proceed from the center of *k*-space and may provide more efficient coverage of *k*-space than radial sampling, although they take longer and this may lead to greater T_2 decay during data collection.

There may also be sequences in which the first echo is of the UTE type but later echoes use a conventional readout so that the sequence as a whole generates both types of image in a single acquisition. The combination of

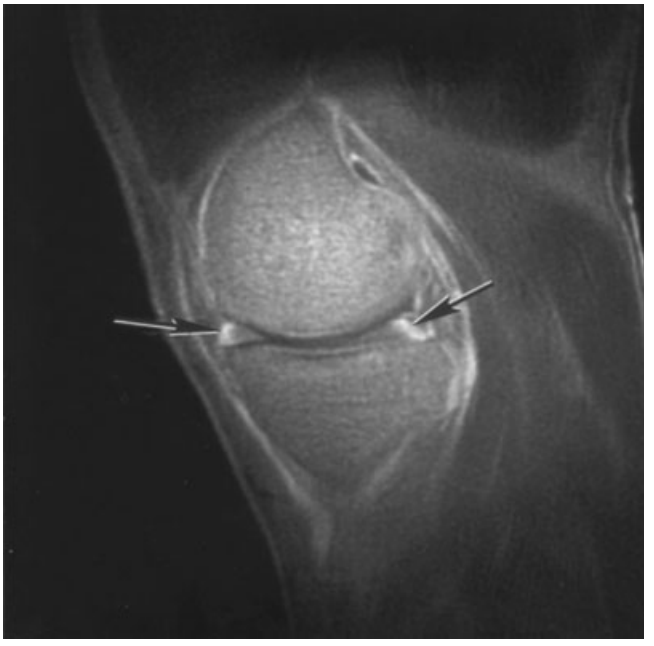

Figure 13. Normal knee meniscus. Sagittal fat-suppressed difference UTE (*TR/TE* = 500/0.08 minus 17 ms) after enhancement. The red (vascular) zone of the meniscus is enhanced (arrows)

Copyright © 2006 John Wiley & Sons, Ltd.

DOI: 10.1002/nbm

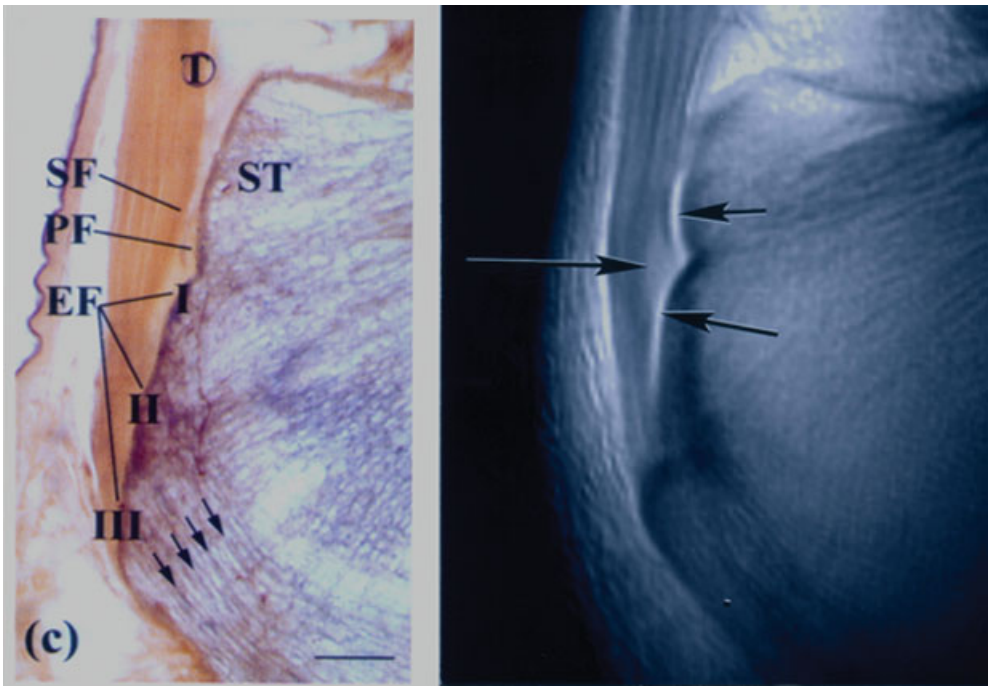

Figure 14. Achilles tendon. Anatomical specimen (left) and UTE image (*TR*/*TE* = 500/0.08 ms) (right). The fibrocartilage in the tendon has a high signal (arrows). The enthesis fibrocartilage (EF), periosteal fibrocartilage (PF) and sesomoid fibrocartilage (SF) are shown with the tendon (T) opposite the superior tuberosity (ST). Arrows show the direction of the trabecular bone

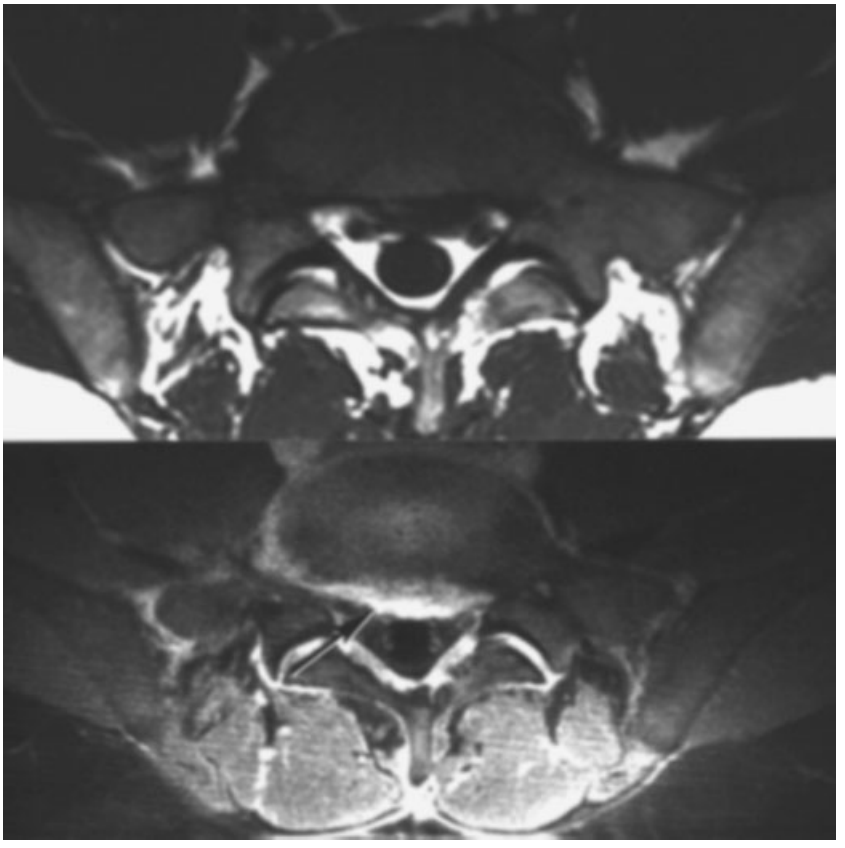

Figure 15. Degenerative disease of the spine. Transverse contrast-enhanced T_1-weighted spin echo (above) and UTE (*TR*/*TE* = 500/0.08 ms) image (below). The disc protrusion (arrow) is more obvious on the UTE image

Copyright © 2006 John Wiley & Sons, Ltd.

DOI: 10.1002/nbm

UTE gradient echoes and spin echoes for the later echoes would also remove some of the susceptibility artifacts that may be present with subtraction from the later gradient echoes. The radial approach is also compatible with partially parallel imaging techniques, given an adequate signal-to-noise ratio. This could allow faster imaging.

Most of this paper has been concerned with the imaging of tissues, but UTE sequences are also useful for the imaging of blood flow since short *TE* decrease the dephasing effects due to flow and can help preserve the signal during turbulence (11).

CONCLUSION

UTE pulse sequences provide a new approach to imaging a group of tissues and tissue components that have previously received little attention in terms of technique development. These sequences detect short T_2 components and are genuinely complementary to conventional sequences such as fast spin echo imaging, EPI and diffusion-weighted imaging which detect long T_2 components. They also detect short T_2 components which cannot be detected with conventional T_1-weighted sequences.

Unlike MR as a whole, which largely proceeded from brain imaging (exploiting its long T_2) to the rest of the body, clinical UTE imaging is likely to proceed initially with tissues with short T_2 in the musculoskeletal system and later to more demanding applications in other systems of the body where short T_2 components are in lower concentration and patient motion is a significant constraint.

Already, tendons, ligaments, menisci, cortical bone and discs have been imaged in novel and interesting ways with and without contrast enhancement, but, as with other developments in clinical MR, UTE sequences will require careful evaluation and detailed comparison with other techniques to establish their clinical role.

Acknowledgments

The authors wish to acknowledge the invaluable help of Atsushi Takahashi, PhD, Ann Shimakawa, PhD, and Jean Brittain, PhD, of Advanced Laboratory Support West (Menlo Park, General Electric), and the assistance of Alexandr Khrapichev, PhD, with the SPRITE sequence.

REFERENCES

1. Smith FW. Clinical application of NMR tomographic imaging. In *NMR Imaging*, Witcofski RL, Karstaedt N, Partain CL (eds). Bowman Gray School of Medicine: Winston Salem, 1982; 25–132.
2. Edelstein WA, Bottomley PA, Hart HR, Leue WM, Schenck JF, Redington RW. In *NMR Imaging*, Witcofski RL, Karstaedt N, Partain CL (eds). Bowman Gray School of Medicine: Winston Salem, 1982; 139–146.
3. Henkelman RM, Stanisz GJ, Graham GJ. Magnetization transfer in MRI: a review. *NMR Biomed*. 2001; **14**: 57–64.
4. Bergin CJ, Pauly JM, Macovski A. Lung parenchyma: projection reconstruction MR imaging. *Radiology* 1991; **179**: 771–781.
5. Bergin CJ, Noll DC, Pauly JM, Glover GH, Macovski A. MR imaging of lung parenchyma: a solution to susceptibility. *Radiology* 1992; **183**: 673–676.
6. Gold G, Pauly J, Moretto J, Glover G, Macovski A, Herfkens R. Characterization of artherosclerotic plaque at 1.5 T. *J. Magn. Reson. Imaging* 1993; **3**: 399–407.
7. Gold GE, Pauly JM, Macovski A, Herfkens RJ. MR spectroscopic imaging of collagen: tendons and knee menisci. *Magn. Reson. Med*. 1995; **34**: 654–674.
8. Brossman J, Frank LR, Pauly JM, Boutin RD, Pedowitz RA, Haghighi P, Resnick D. Short echo time projection reconstruction MR imaging of cartilage with histopathologic correlation: comparison with fat-suppressed spoiled GRASS and magnetization transfer contrast MR imaging. *Radiology* 1997; **203**: 501–507.
9. Schmidt MA, Yang GZ, Gatehouse PD, Firmin DN. FID-based lung MRI at 0.5 T: theoretical considerations and practical implications. *Magn. Reson. Med*. 1998; **39**: 666–672.
10. Gold GE, Thedens DR, Pauly JM, Fechner KP, Bergman G, Beaulieu CF, Macovski A. MR imaging of the articular cartilage of the knee: new methods using ultrashort TEs. *Am. J. Roentgenol. AJR* 1998; **170**: 1223–1226.
11. Neilson HT, Gold GE, Olcott EW, Pauly JM, Nishimura DG. Ultrashort echo time 2D time of flight MR angiography using a half-pulse excitation. *Magn. Reson. Med*. 1999; **41**: 592–599.
12. Nayak KS, Pauly JM, Gold GE, Nishimura DG. Imaging ultrashort T2 species in the brain. *Proc. Int. Soc. Magn. Reson. Med*. 2000; 509.
13. Gold GE, Wren TAL, Nayak KS. In vivo short echo time imaging of Achilles Tendon. *Proc. Int. Soc. Magn. Reson. Med*. 2001; 244.
14. Gold GE, Pauly JM, Leung AN, Block WF, Meyer CH, Sze R, Macovski A, Stark P. Short echo time MR spectroscopic imaging of the lung parenchyma. *J. Magn. Reson. Imaging* 2002; **15**: 679–684.
15. Lu A, Grist TG, Black WF. Improved spectral selectivity and reduced susceptibility in true-FISP using a near zero TE undersampled 3D PR sequence. *Proc. Int. Soc. Magn. Reson. Med*. 2002; 470.
16. Gatehouse PD, Bydder GM. Magnetic resonance imaging of short T2 components in tissues. *Clin. Radiol*. 2003; **58**: 1–19.
17. Chappell KE, Patel N, Gatehouse PD, Main J, Puri BK, Taylor-Robinson SD, Bydder GM. Magnetic resonance imaging of the liver with ultrashort TE (UTE) pulse sequences. *J. Magn. Reson. Imaging* 2003; **18**: 709–713.
18. Waldman A, Rees JH, Brock CS, Robson MD, Gatehouse PD, Bydder GM. MRI of the brain with ultra-short echo-time pulse sequences. *Neuroradiology* 2003; **45**: 887–892.
19. Robson MD, Gatehouse PD, Bydder M, Bydder GM. Magnetic resonance: an introduction to ultrashort TE (UTE) imaging. *J. Comput. Assist. Tomogr.* 2003; **27**: 825–846.
20. Hall-Craggs MA, Porter J, Gatehouse PD, Bydder GM. Ultrashort echo time (UTE) MRI of the spine in thalassaemia. *Br. J. Radiol*. 2004; **77**: 104–110.
21. Reichert IL, Benjamin M, Gatehouse PD, Chappell KE, Holmes J, He T, Bydder GM. Magnetic resonance imaging of periosteum with ultrashort TE pulse sequences. *J. Magn. Reson. Imaging* 2004; **19**: 99–107.
22. Robson MD, Gatehouse PD, So PW, Bell JD, Bydder GM. Contrast enhancement of short T2 tissues using ultrashot TE (UTE) pulse sequences. *Clin. Radiol*. 2004; **59**: 720–726.
23. Robson MD, Benjamin M, Gishen P, Bydder GM. Magnetic resonance imaging of the Achilles tendon using ultrashort TE (UTE) pulse sequences. *Clin. Radiol*. 2004; **59**: 727–735.
24. Chung CB, Dwek JR, Haghighi P, Puni R, Bydder GM. Ultrashort TE imaging evaluation of the femorotibial and patellofemoral cartilage of the knee: imaging comparison with histology in 10 cadaveric specimens to establish the normal and pathologic MR appearance of the deep layer of articular cartilage. *Proc. Radiological Society of North America* 2004; 463.
25. Turner R, Benjamin M, Bydder M, Robson MD, Bydder GM. Visualization of entheses with ultrashort TE (UTE) pulse sequences. *Proc. Int. Soc. Magn. Reson. Med*. 2004; 174.

Copyright © 2006 John Wiley & Sons, Ltd.

DOI: 10.1002/nbm

26. Brittain J, Shankaranarayanan A, Ramanan V, Shimakawa A, Cunningham C, Hinks S, Francis R, Turner R, Johnson J, Nayak K, Tan S, Pauly J, Bydder GM. Ultra-short TE imaging with single-digit (8 μs) TE. *Proc. Int. Soc. Magn. Reson. Med*. 2004; 629.
27. Schroeder C, Boernert P, Rahmer J. Slice excitation for ultrashort TE imaging. *Proc. Int. Soc. Magn. Reson. Med*. 2004; 628.
28. Robson MD, Gatehouse PD, Bydder GM, Neubauer S. Human imaging of phosphorus in cortical and trabecular bone in vivo. *Magn. Reson. Med*. 2004; **51**: 888–892.
29. Schroeder C, Rahmer J, Bornert P, Leussler C. Scan time reduction for ultrashort TE imaging at 3 T. *Proc. Int. Soc. Magn. Reson. Med*. 2004; 137.
30. Gatehouse PD, Thomas RW, Robson MD, Hamilton G, Herlihy AH, Bydder GM. Magnetic resonance imaging of the knee with ultrashort TE pulse sequences. *Magn. Reson. Imaging* 2004; **22**: 1061–1067.
31. Reichert IL, Robson MD, Gatehouse PD, He T, Chappell KE, Holmes J, Girgis S, Bydder GM. Magnetic resonance imaging of cortical bone with ultrashort TE pulse sequences. *Magn. Reson. Imaging* 2005; **23**: 611–618.
32. Bydder M, Robson M, Gatehouse P, Znamirowski R, Benjamin M, Bydder GM. Magnetic resonance imaging: improved visualization of bone with ultrashort TE (UTE) pulse sequences. *Proc. Int. Soc. Magn. Reson. Med*. 2005; 1989.
33. Takahashi A, Lu A, Brittain J, Hinks S, Shimakawa A, Johnson J, Cunningham C, Block W, Pauly J, Bydder GM. Ultra-short TE (UTE) imaging at 8 μsec with 3D vastly undersampled isotropic projection reconstruction (VIPR). *Proc. Int. Soc Magn. Reson. Med*. 2005; 2405.
34. Rahmer J, Bornert P, Grasslin I, Overweg J, Mazurkewitz P, Winkelmann R. 3D ultrashort echo-time imaging using a 32 channel receiver array. *Proc. Int. Soc. Magn. Reson. Med*. 2005; 795.
35. Rahmer J, Bornert P, Eggers H. 3D ultrashort echo-time imaging of the head. *Proc. Int. Soc. Magn. Reson. Med*. 2005; 1074.
36. Rahmer J, Bornert P. Effects of T2 decay on the point-spread function for 3D radial FID sampling. *Proc. Int. Soc. Magn. Reson. Med*. 2005; 2354.
37. Mentrup D, Eggers H. Iterative signal decay correction: application to 2D ultra-short TE imaging. *Proc. Int. Soc. Magn. Reson. Med*. 2005; 2291.
38. Larson PE, Vidarsson L, Pauly JM, Nishimura DG. Linear combination filter long-T2* suppression in ultra-short echo time (UTE) imaging. *Proc. Int. Soc. Magn. Reson. Med*. 2005; 2264.
39. Crowe L, Wang Y, Gatehouse P, Tessier J, Waterton J, Robert P, Bydder GM, Firmin D. Ex vivo MR imaging of atherosclerotic rabbit aorta labelled with USPIO–enhancement of iron loaded regions in UTE imaging. *Proc. Int. Soc. Magn. Reson. Med*. 2005; 115.
40. Larson PE, Pauly JM, Nishimura DG, Conolly SM. Using adiabatic inversion pulses to suppress long-T2 species in ultra-short echo time (UTE) imaging. *Proc. Int. Soc. Magn. Reson. Med*. 2005; 786.
41. Larson PE, Nishimura DG, Pauly JM. Designing long-T2 and combination long-T2/fat suppression pulses for ultra-short echo time (UTE) imaging. *Proc. Int. Soc. Magn. Reson. Med*. 2005; 2345.
42. Robson MD, Tyler DJ, Neubauer S. Ultrashort TE chemical shift imaging (UTE-CSI). *Magn. Reson. Med*. 2005; **53**: 267–274.
43. Does MD, Snyder RE. T2 relaxation of peripheral nerve measured in vivo. *Magn. Reson. Imaging* 1995; **13**: 575–580.
44. MacKay A, Whittall K, Adler J, Li D, Paty D, Graeb D. In vivo visualization of myelin water in brain by magnetic resonance. *Magn. Reson. Med*. 1994; **31**: 673–677.
45. Fenrich FR, Beaulieu C, Allen PS. Relaxation times and microstructures. *NMR Biomed*. 2001; **4**: 133–139.
46. Henkelman RM, Stanisz GJ, Kim JK, Bronskill MJ. Anisotropy of NMR properties of tissue. *Magn. Reson. Med*. 1994; **32**: 592–602.
47. Hayes CW, Parellada JA. The magic angle effect in musculoskeletal MR imaging. *Top Magn. Reson. Imaging* 1996; **8**: 51–56.
48. Oatridge A, Herlihy AH, Thomas RW, Wallace AL, Curati WL, Hajnal JV, Bydder GM. Magnetic resonance: magic angle imaging of the Achilles tendon. *Lancet* 2001; **358**: 1610–1611.
49. Oatridge A, Herlihy A, Thomas RW, Wallace AL, Puri BK, Larkman DJ, Bydder GM. Magic angle imaging of the Achilles tendon in patients with chronic tendonopathy. *Clin. Radiol*. 2003; **58**: 384–388.
50. Bydder M, Brittain J, Shimakawa A, Takahashi A, Johnson J, Robson MD, Znamirowski R, Bydder GM. Magic angle effects and ultrashort TE (UTE) imaging. *Proc. Int. Soc. Magn. Reson. Med*. 2005; 586.
51. Krasnosselskaia LV, Fullerton GD, Dodd SJ, Cameron FL. Water in tendon: orientational analysis of the free induction decay. *Magn. Reson. Med*. 2005; **54**: 280–288.
52. Fullerton GD, Nes E, Amurao M, Rahal A, Krasnosselkaia L, Cameron I. An NMR method to characterize multiple water compartments on mammalian collagen. *Cell Biol. Int*. 2006; **30**: 63–73.
53. Harrison R, Bronskill MJ, Henkelman RM. Magnetization transfer and T2 relaxation components in tissue. *Magn. Reson. Med*. 1995; **33**: 490–496.
54. Pauly J, Conolly S, Macovski A. Suppression of long T2 components for short T2 imaging. *J. Magn. Reson. Imaging* 1992; 145.
55. Brown TR, Kincaid BM, Ugurbil K. NMR chemical shift imaging in three dimensions. *Proc. Natl Acad. Sci USA* 1982; **79**: 3523–3526.
56. Enid S, Creyghton JHN. High resolution NMR imaging in solids. *Physica* 1985; **125B**: 81–83.
57. Cho ZH, Ro YM. Multipoint K-space point mapping (KPM) technique for MR microscopy. *Magn. Reson. Med*. 1994; **32**: 258–261.
58. Balcom BJ, Macgregor RP, Beyea SD, Green DP, Armstrong KL, Brenner TW. Single-point ramped imaging with T1 enhancement (SPRITE). *J. Magn. Reson*. 1996; **123**: 31–34.
59. Fernandez-Seara MA, Wehrli SL, Wehrli FW. Multipoint mapping of semi-solid materials. *J. Magn. Reson*. 2003; **160**: 144–150.
60. Idiyatullin D, Corum C, Park J-Y, Garwood M. Fast and quiet MRI using a swept radiofrequency. *J. Magn. Reson*. 2006; **181**: 342–349.
61. Halse M, Rioux J, Romanzetti S. Centric scan SPRITE magnetic resonance imaging: optimization of SNR, resolution, and relaxation time mapping. *J. Magn. Reson*. 2004; **169**: 102–117.
62. Mastikhin II, Balcom BJ, Prodo PJ, Fennedy CB. SPRITE MRI with prepared magnetization and centric *k*-space sampling. *J. Magn. Reson*. 1999; **36**: 59–68.
63. Romanzetti S, Halse M, Kaffanke J, Zilles K, Balcom BJ, Shah NJ. A comparison of three SPRITE techniques for the quantitative 3D imaging of the (23)Na spin density on a 4 T whole-body machine. *J. Magn. Reson*. 2006; **179**: 64–72.
64. Connolly S, Nishimura D, Macovski A. Variable rate slice-selective excitation. *J. Magn. Reson*. 1988; **78**: 440–457.
65. Robson MD, Gatehouse P, Young I, Bydder GM. Ultrashort TE (UTE) imaging of short T2 relaxation components: How should the T2 weighting be described? *Proc. Int. Soc. Magn. Reson. Med*. 2004; 636.
66. Sussman MS, Pauly JM, Wright GA. Design of practical T2 sensitive rf excitation (TELEX) pulses. *Magn. Reson. Med*. 1998; **40**: 890–899.
67. Hauger O, Frank LR, Boutin RD, Lektrakul N, Chung CB, Haghighi P, Resnick D. Characterization of the 'red zone' on knee meniscus: MR imaging and histologic correlation. *Radiology* 2000; **217**: 193–200.
68. Benjamin M, Ralphs JR. Fibrocartilage in tendons and ligaments – an adaptation to compressive load. *J. Anat*. 1998; **193**: 481–494.

Copyright © 2006 John Wiley & Sons, Ltd.

DOI: 10.1002/nbm